

---

# TARGET TO SOURCE: GUIDANCE-BASED DIFFUSION MODEL FOR TEST-TIME ADAPTATION

---

Kaiyu Song, Hanjiang Lai  
Sun Yat-Sen University  
{songky7, laihanj3}@mail.sysu.edu.cn

## ABSTRACT

Most recent works of test-time adaptation (TTA) aim to alleviate domain shift problems by re-training source classifiers in each domain. On the other hand, the emergence of the diffusion model provides another solution to TTA, which directly maps the test data from the target domain to the source domain based on a diffusion model pre-trained in the source domain. The source classifier does not need to be fine-tuned. However, 1) the semantic information loss from test data to the source domain and 2) the model shift between the source classifier and diffusion model would prevent the diffusion model from mapping the test data back to the source domain correctly. In this paper, we propose a novel guidance-based diffusion-driven adaptation (GDDA) to overcome the data shift and let the diffusion model find a better way to go back to the source. Concretely, we first propose detail and global guidance to better keep the common semantics of the test and source data. The two guidance include a contrastive loss and mean squared error to alleviate the information loss by fully exploring the diffusion model and the test data. Meanwhile, we propose a classifier-aware guidance to reduce the bias caused by the model shift, which can incorporate the source classifier’s information into the generation process of the diffusion model. Extensive experiments on three image datasets with three classifier backbones demonstrate that GDDA significantly performs better than the state-of-the-art baselines. On CIFAR-10C, CIFAR-100C, and ImageNetC, GDDA achieves 11.54%, 19.05%, and 11.63% average accuracy improvements, respectively. GDDA even achieves equal performance compared with methods of re-training classifiers. The code is available in the supplementary material.

## 1 Introduction

Deep neural networks (DNNs) achieve great success in various vision tasks such as image classification [1] and face recognition [2]. However, DNNs suffer from the domain shift problem [3] where the distribution of test data is different from that of the train data. The phenomenon of data shift is common and can be caused by various factors such as the corruption [4], the adversarial perturbation [5], and the differences in styles and backgrounds [6]. Test-time adaptation (TTA) [3] is one of the main paradigms for the domain shift problem. TTA has various settings including test-time training [7] and fully test-time adaptation [8, 3, 9, 10, 11].

Contemporary mainstream TTA approaches use *source-to-target methods* [7, 8, 10, 9, 3] to fine-tune the classifier pre-trained in the source domain at the test time. For example, Zhang *et al.* [7] proposed the test-time augmentation method (MEMO). Wang *et al.* [3] proposed TENT, an initial framework of the entropy-based method. While source-to-target methods suffer from two main problems. One is that fine-tuning the source model can result in catastrophic forgetting [12], which can harm the performance in the source domain [3]. In such cases, it is necessary to train a specific model for each domain. The other one is sensitive to the settings including the model type, the hyperparameters [13], and the settings [4].

In contrast, another genre, known as the *target-to-source method*, has emerged in recent studies [4]. In this approach, the goal is to directly map the test image from the target domain to the source domain, thus avoiding the need for fine-tuning the source model. This approach draws inspiration from the success of diffusion models [14] in generating images. We only require a pre-trained diffusion model in the source domain. In diffusion-driven adaptation (DDA) [4], there are two steps involved: 1) during training, a diffusion model is trained using the source data, and a classifier is

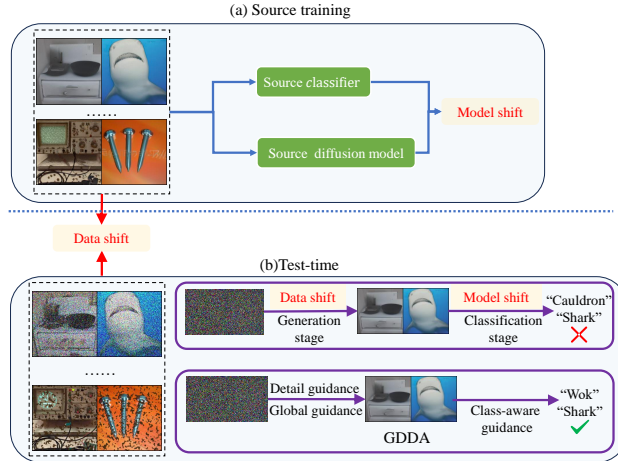


Figure 1: An illustration of GDDA. Given the pre-trained diffusion model and classifier, (a) identifies two weaknesses: data shift and model shift. (b) shows the data shift caused by Gaussian noise, which disturbs some of the meaningful information in the image during the generation stage. Meanwhile, (b) also shows the model shift during the classification stage. These weaknesses impede the reverse process of returning from the source domain to the target domain. GDDA aims to address the two weaknesses by leveraging three guidance based on the source diffusion model and classifier.

trained with the labeled source data; 2) during inference, the test image is projected onto the source domain, and the fixed classifier is used to recognize the projected image. However, the performance of this method typically lags behind the performance of source-to-target methods.

This paper aims to improve target-to-source methods in the paradigm by providing a more effective approach to return to the source as shown in Figure 1. We have identified two potential weaknesses that may impact the correct mapping: 1) semantic information loss caused by the data shift between the source data and the test data. Since the diffusion model is trained only on the source domain, mapping the unseen test data back to the source domain will inevitably lose the semantic information and have a bad influence on the reverse generative process of the source diffusion model. DDA [4] proposed a low-frequency filter to preserve the semantic information. However, it still suffers from the loss of the label semantic since the low-frequency filter itself will drop the feature of the high-frequency part; 2) The model shift between the source classifier and diffusion model. The generated good quality images from the diffusion model do not always have good performance of the classifier, e.g., all test images are mapped to one class. In DDA [4], the diffusion model and the classifier are used in different steps and are independent. The target of TTA is to correctly recognize the generated images using the source classifier. It is desired to combine the classifier into the generated process of the diffusion model.

To alleviate these, we propose a novel guidance-based diffusion-driven adaptation (GDDA). Following the setting of the DDA, we focus on the test-time corruption. The key to the success of GDDA is that we leverage the feature maps from the diffusion model and the test data to effectively reduce the data shift of the target domain. Meanwhile, we continue to leverage the property of feature maps within the source classifier. In this scenario, we incorporate the classifier as the guidance into the reverse process, which further reduces the gap between the diffusion model and the classifier.

Concretely, to alleviate the semantic information loss caused by data shift, we propose the contrastive loss [15] based guidance (Detail guidance) to keep the details as much as possible by leveraging the representation of the diffusion model. Motivated by the Zecon[16], we propose an effective aggregating method to leverage the feature maps and implement the contrastive loss based on the aggregated feature maps. Meanwhile, we use mean squared error (MSE) based guidance (Global guidance) as a regularization term to keep the global features between the test data and the generated sample simultaneously. Then, to alleviate the model shift between the classifier and the diffusion model, inspired by the LPIPS [17], we propose the class-aware guidance, where we prove that LPIPS could be used to reduce the model shift. Since there is too much noise during the early phase of the diffusion model, we propose an additional sampling strategy to decide when to start in the adaptive way. In the end, the experimental results show that GDDA achieves state-of-the-art results, where GDDA gets a large improvement compared with previous target-to-source methods and is close to the source-to-target methods.

To sum up, the main contributions of this paper are:

- We have proposed GDDA, a guidance-based diffusion-driven adaptation method that aims to address two weaknesses in the same setting as DDA. Based on the proposed three novel guidance, GDDA effectively bridges the gap caused by data shift and model shift.
- We highlight that the guidance-based diffusion model holds great potential for adapting to domain shifts during test time. By designing the guidance based on a pre-trained diffusion model, it becomes possible to address a wide range of domain shift problems caused by corruption.
- The experimental results show that GDDA achieves state-of-the-art results via various target-to-source methods. It even achieves comparable or superior performance when compared with source-to-target methods.

## 2 Related Work

**Source-to-target methods.** In the TTA setting, the parameter-based method aims to utilize the unlabeled target data in order to fine-tune the model’s parameter. Specifically, to handle the unlabeled situation, the test-time train [8] has been proposed by creating an auxiliary task to automatically label the target data, e.g., predicting the rotation angle. Then a full test-time adaptation by entropy minimization [3], an entropy-based TTA method, has been further proposed in fully test-time adaptation setting. Nguyen [9] further proposed to leverage the transformation invariance such that it drops the training procedure in TENT to achieve the complete fully test-time adaptation. However, Zhao *et al.* proved that parameters-based methods are inevitably influenced by the hyperparameter settings, e.g., batch size, and harness the performance of the classifier.

**Target-to-source methods.** It focuses on using a generative model trained from the source domain to map the target images from the target domain to the source domain for corruption shift. The closest one is DiffPure [18] which uses the diffusion model against the shift caused by the adversarial perturbation. Following this, Gao *et al.* [4] leverage the diffusion model to alleviate the domain shift caused by the corruption based on the guidance method with a low-frequency filter. However, using a low-frequency filter alone is insufficient to preserve semantic information caused by the data shift. Meanwhile, model shift can cause slight changes in the generated image, which can result in incorrect classification. In this condition, there is a gap between the performance of source-to-target method and that of target-to-source methods. To address this gap, we propose GDDA with multiple guidance to overcome the semantic information loss caused by data shift and model shift.

**Guidance-based diffusion model.** Based on the unconditional generation of the diffusion model such as DDPM [14], the guidance-based diffusion models have been proposed. For example, Chung *et al.* [19, 20] proposed the train-free guidance by leveraging the gradient of a loss function based on the assumption that the inputs follow the Gaussian distribution. To loosen this assumption, Tumanyan *et al.* [21] indicates that a differentiable loss is all we need to implement the train-free guidance. Following this, Yang *et al.* [16] utilizes various differentiable losses to achieve the style-transfer takes with high quality and stability. The ability of the guidance-based diffusion models shows the potential ability to solve the domain shift since there are similarities between the domain shift and style-transfer tasks.

## 3 Preliminary

**Problem formation.** Following the settings of previous target-to-source methods: the source data could be only used to pre-train the diffusion model and the source classifier. Hence, the pre-trained source classifier  $p_\phi(y|x)$  and the pre-trained diffusion model  $f_\theta$  are available. However, the source data is not available during test time. The test data in the target domain is represented as  $X^{TT}$ . The target-to-source method aims to alleviate the domain shift without fine-tuning the classifier by projecting the test data back to the source domain.

**Target-to-source methods based on the diffusion model.** In order to make the test data be generated back to the source data, DDA [4] used the source data to train the diffusion model. The data in the source domain is represented as  $X^S$ . It will firstly train a diffusion model  $\epsilon_\theta(x_t, t)$  [14] using the source data, where  $\epsilon_\theta(\cdot, \cdot)$  is the score function [22] based on the parameters  $\theta$  in the pre-trained diffusion model.

With the score function  $\epsilon_\theta(x_t, t)$ , given data  $x \in X^{TT}$ , the  $x$  is mapped to the pure Gaussian noise in the forward process:

$$x_t = \sqrt{\sigma(t)}x + \sqrt{(1 - \sigma(t))}\epsilon \quad (1)$$

where  $x_t$  is the state in the  $t$  time,  $\sigma(\cdot)$  is the noise schedule related to the time step  $t$ , and  $\epsilon \sim \mathcal{N}(0, 1)$  is the Gaussian noise.

Then  $x_t$  is implemented via the reverse process [14]:

$$x_{t-1} = \frac{1}{\sqrt{1 - \beta_t}} \left( x_t - \frac{\beta_t}{\sqrt{1 - \sigma(t)}} \epsilon_\theta(x_t, t) \right) + \phi_t * \epsilon, \quad (2)$$

where  $\beta_t$  and  $\phi_t$  are the calculated parameters of the noise schedule related to the time step  $t$  respectively.

Since the diffusion model is trained on the source data  $X^S$ , the generated image  $x_0$  will gradually become close to the source distribution. But it would cause the semantic information loss of test data.

**Data shift.** In the target-to-source methods, we have to keep the semantics of test data during the reverse process. As a train-free method, the guidance method [19] is a popular choice. In this method, the target data  $x^{TT}$  is used as the guidance to project the target data back to the source domain formulated in Bayesian framework [19]:

$$p(x_t | x^{TT}) = \underbrace{\epsilon_\theta(x_t, t)}_{\text{Score Function}} + \underbrace{\nabla_x \log p(x^{TT} | x; t)}_{\text{Guidance Term}}. \quad (3)$$

Following the Chung *et al.* [19], the guidance term could be calculated:

$$\nabla_x \log p(x^{TT} | x; t) \approx -\frac{1}{\sigma(t)^2} \nabla_{x_t} \ell_2(\hat{x}_t, x^{TT}), \quad (4)$$

where  $\ell_2(\cdot, \cdot)$  is the distance metric and  $\hat{x}_t$  is the estimation for  $x_0$  based on the  $t$  time step [19]:

$$\hat{x}_t \approx \frac{1}{\sqrt{\sigma(t)}} (x_t + (1 - \sigma(t)) * \epsilon_\theta(x_t, t)). \quad (5)$$

When the target and source data have the same data distribution, the term  $\ell_2(\hat{x}_t, x^{TT})$  can accurately calculate the distance between  $\hat{x}_t$  and  $x^{TT}$ . The diffusion model could benefit from incorporating accurate distance measurements to preserve the details of the inputs. In test-time adaptation, domain shift can result in data shift, which includes changes in the label semantics of  $x^{TT}$ . This will cause an error for calculating  $\ell_2(\hat{x}_t, x^{TT})$  and result in loss of target information.

Previous methods tackled the error by incorporating a low-frequency filter [4]  $f_{low}(\cdot)$ , which is based on the Fourier transform. It captures the structure of the image at the pixel level in order to compensate for loss of target information, which is defined as:

$$\ell_2(\hat{x}_t, x^{TT}) \approx \|f_{low}(\hat{x}_t) - f_{low}(x^{TT})\|_2^2. \quad (6)$$

However, there is a strong assumption with the low-frequency filter to make sure it captures the image-level structure without the loss and this assumption may not be satisfied during test-time adaptation.

**Model shift.** The target of the diffusion model is to learn the data distribution  $p(x; \theta)$  with  $\theta$  as the set of parameters for  $\epsilon_\theta$ . In contrast, the target of the classifier is to learn  $p(y; \phi)$ , where  $y$  is the label for the  $x$ ,  $\phi$  is the set of the parameters of the classifier  $p_\phi(y|x)$ , and the difference could be defined as:

**Proposition 1.** *The Kullback–Leibler (KL) divergence between the generative model and the discriminative model not equal to 0.*

$$KL(p(x; \theta) || p(y|x; \phi)) > \zeta, \quad (7)$$

where  $\zeta$  is the non-zero constant.

Proposition 1 is from the difference between the discriminative model and the generative model. It is clear that there is a model shift between the classifier and the diffusion model.

## 4 Method

In this paper, we adopt the settings of the target-to-source methods, where we only have a pre-trained source classifier and a pre-trained source diffusion model [14] for test-time adaptation. Given a test image  $x^{TT}$ , we will begin with a random Gaussian noise  $x_T$  and iteratively follow the reverse steps to generate the  $x_0$ . In each reverse step, the test image  $x^{TT}$  is used as a guidance. Please note the source diffusion model and classifier are frozen at test time.

To alleviate the two weaknesses, we propose three guidance: *detail guidance*, *global guidance*, and *classifier-aware guidance*, abbreviated as  $\{g^1, g^2, g^3\}$ , to map the  $x^{TT}$  from the target domain to the source domain. And then the source classifier could classify  $x^{TT}$  correctly. The  $g = \{g^1, g^2, g^3\}$  are defined as:

$$g^i = \nabla_x \log p^i(x^{TT} | x; t). \quad (8)$$

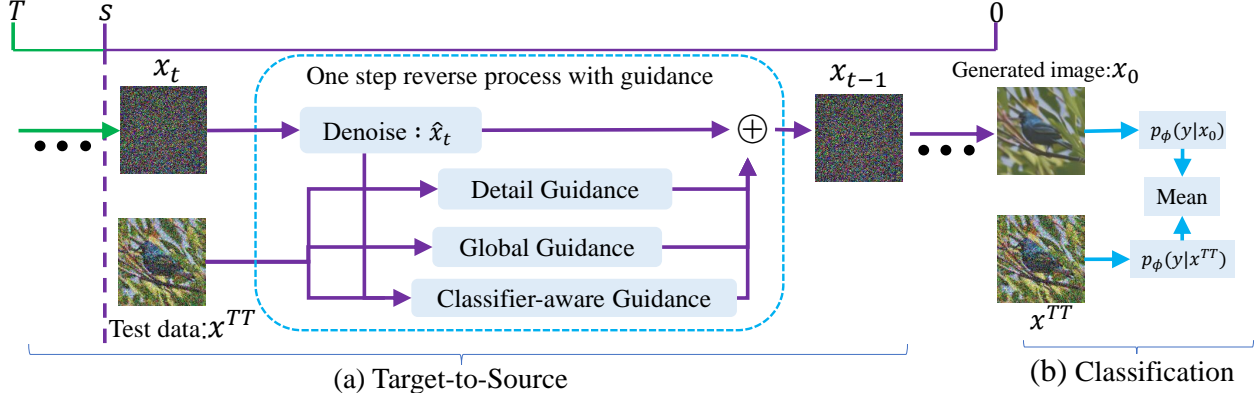


Figure 2: An overview of the proposed GDDA, where denoise is to estimate the  $\hat{x}_t$ . We implement the guidance method in the interval  $t \in [s, 0)$ , and the interval  $t \in [T, s)$  is the reverse process without guidance.  $x_t \rightarrow x_{t-1}$  represents the one step of the reverse process after implementing the guidance method. We first achieve target-to-source process (a) to generate the  $x_0$  and use both  $x_0$  and  $x^{TT}$  to finish the classification (b).

The overall method is shown in Fig 2.

**Detail guidance.** To leverage the test data, we first propose the detail guidance. The main challenge is that the diffusion model is only trained on the source data. Thus, the source diffusion model has limitations in preserving the information of the unseen test data. To preserve more detailed information of test data, we use patch-wise contrastive loss [15] inspired by the style transfer [15] that can effectively preserve structural information of images.

At the reverse timestep  $t$ , we use the source diffusion model  $f_\theta(\cdot, t)$  to extract the features for the generated image  $x_t$  and the guided image  $x^{TT}$ . Our work further shows that the diffusion model could extract spatial features even in the TTA situation and has the potential to achieve all back to the source without any fine-tuning on the target domain, which is an additional contribution to this work. Meanwhile, we argue that using all feature maps from the source diffusion model does not work well [16]. The reason is that the guided image  $x^{TT}$  is from another test domain, where domain-specific information should be reduced. Using all embedding features may intensify the domain-specific information and ignore the common parts. Therefore, we propose an aggregation strategy for preserving more common information.

Specifically, for each image, we first use the  $f_\theta(\cdot, t)$  to extract the feature maps  $E \in \mathbb{R}^{C \times H \times W}$ , where  $C$  is the channel and  $(H, W)$  is the resolution of the feature maps. Suppose the number of the layers in UNet of  $f_\theta(\cdot, t)$  is  $L$ , then we can obtain  $L$  feature maps with different channels, heights, and widths. According to the channels, we split the  $L$  feature maps into  $M$  groups:  $\{G_1, G_2, \dots, G_M\}$ , where each group has the same number of channels, and  $G_m$  is the number of layers in the  $m$ -th group with  $\sum_{m=1}^M G_m = L$ .

For the  $G_m$  group, the number of channels for all feature maps is the same, denoted as  $C_m$ . We denote the minimum resolution as  $(H_m^{\min}, W_m^{\min})$ . We reshape all the feature maps in the  $G_m$  group into  $E'_m \in \mathbb{R}^{C_m \times H_m^{\min} \times W_m^{\min}}$ . After reshaping, all the feature embedding in the same group have the same channel and resolution. We finally use the sum operator to sum the feature maps in the same group followed by a batch norm layer, denoted as  $\hat{E}_m$ , where  $\hat{E}_m = \text{BatchNorm}(\sum_{E \in E'_m} E)$ .

We use the sum operator to capture the common features in each group. The common features would frequently appear in different layers and thus sum operator can intensify the common signal. The batch norm layer is used to smooth the gradient required by the guidance method. The  $\hat{E}_m$  is the aggregated embedding feature.

In the end, similar to the ViT [23] which divides the image into  $P \times P$  patches, we reshape the  $\hat{E}_m \in \mathbb{R}^{C_m \times H_m^{\min} \times W_m^{\min}}$  into 2D sequence patches  $e_m^p$  [23]. Based on the embedding feature patches extracted from  $x^{TT}$  and  $\hat{x}_t$ , we build the pairs:  $\{(e_1^{p,1}, e_1^{p,2}), \dots, (e_m^{p,1}, e_m^{p,2})\}$ , where  $e_m^{p,1}$  denotes the patch from  $x^{TT}$  and  $e_m^{p,2}$  denotes the patch from  $\hat{x}_t$  respectively. For each pair, we calculate the patch-aware contrastive loss:

$$\ell_{cl}(e_m^{p,1}, e_m^{p,2}) = \frac{\exp(s_{i,i}/\tau)}{\sum_{k \neq i} \exp(s_{i,k}/\tau) + \exp(s_{i,i}/\tau)}, \quad (9)$$

where  $s_{i,i}$  is the patch-aware similarity matrix related to pair  $(e_m^{p,1}, e_m^{p,2})$  [24].

Therefore, the detail guidance could be calculated based on all embedding feature patches as:

$$\begin{aligned} g^1 &= \nabla_x \log p^1(x^{TT}|x; t) \\ &= \nabla_{x_t} \frac{1}{M} \sum_{i=1}^M \ell_{cl}(e_i^{p,1}, e_i^{p,2}). \end{aligned} \quad (10)$$

**Global guidance.** Inspired by [16], contrastive loss will fall into the local feature and ignore part of the global information. Hence, we use the MSE to keep the global information. MSE could measure the absolute distance for each pixel and thus could be regarded as the regularization term to keep the global information such as style [16], which is calculated as:

$$\begin{aligned} g^2 &= \eta \nabla_x \log p^2(x^{TT}|x; t) \\ &= \eta \nabla_{x_t} \|x^{TT} - \hat{x}_t\|_2^2, \end{aligned} \quad (11)$$

where  $\eta$  is the constant to weaken the weight of the MSE loss.

**Classifier-aware guidance.** Given the pre-trained source classifier  $\phi$ , the point estimation for an input  $x$  is  $p_\phi(y|x)$  [25]. The  $p_\phi(y|x)$  depends on the extracted features that have a high probability of being classified correctly. These efficient features are needed to be kept during the generation. However, Proposition 1 will lead to the diffusion model slightly changing and dropping part of the efficient features, which causes the model shift. To address this issue, we propose to use the pre-trained source classifier to extract efficient features during the test-time adaptation. The source classifier is widely used in the source-to-target methods, e.g., the entropy-based source-to-target methods [3] utilize the entropy to refine the source classifier and decrease its uncertainty by minimizing the overall entropy. In this scenario, the efficient features that have a high level of certainty for classification can be preserved in the generation process. Please note that the source classifier is fixed in our method.

Based on this, we want to leverage the efficient features hidden in the classifier to alleviate the model shift. Therefore, we first extract the features from the classifier  $\phi$ , and obtain the features for  $\hat{x}_t$  and  $x^{TT}$ , respectively. However, the data shift causes semantic information loss. This will introduce the bias if we use a simple metric such as MSE. Motivated by the LPIPS [17], perceptual similarity refers to the way humans perceive visually. This property of human perception can be utilized to retain common features through the use of feature maps. Humans can easily adapt to different styles (for example, we can quickly and accurately recognize a house in both cartoon style and realistic style). Therefore, we use  $\phi(\cdot)$  as the feature mapping function and propose the LPIPS-based guidance:

$$\begin{aligned} g^3 &= \nabla_x \log p^3(x^{TT}|x; t) \\ &= \nabla_{x_t} \ell_{Lpips}(\phi(x^{TT}), \phi(\hat{x}_t)), \end{aligned} \quad (12)$$

where  $\ell_{Lpips}$  is the LPIPS-based distance metric and  $\phi(x)$  is the features of all layers before the classification layer.

**Sampling strategy.** In the early phase,  $\hat{x}_t$  is close to the pure Gaussian noise, which will lead to much bias when calculating guidance. Meanwhile, the acceleration method such as DPM-Solver++ [26] is sensitive to the bias. To avoid these problems and let GDDA be implemented in accelerating methods (DPM-Solver++) directly, following the empirical finding [27], it is better to implement the guidance method in the latter phase, which is defined as the interval  $[s, 0)$ . Finding  $s$  is a complex task, and thus we use an upper bound to indicate the beginning of the guidance method rather than calculate a specific value for  $s$ . In the early phase,  $\hat{x}_t$  have much Gaussian noise and largely increase the MSE loss between  $\hat{x}_t$  and  $x^{TT}$ . We think the image contains no useful semantic information when the MSE between  $\hat{x}_t$  and  $x^{TT}$  is larger than that between pure white image/pure black image and  $x^{TT}$  and to keep that  $\hat{x}_t$  is an image with some sensitive object instead of the pure Gaussian noise at least. Therefore, the  $s$  is the time satisfied :

$$\|\hat{x}_s - x^{TT}\|_2^2 \leq \max(\|x^{blk} - x^{TT}\|_2^2, \|x^{whi} - x^{TT}\|_2^2), \quad (13)$$

where  $x^{blk}$  is the pure black image with all pixels to be 0 and  $x^{whi}$  is the pure white image with all pixels to be 1.

Meanwhile, to leverage the prior knowledge of the classifier from the target domain, we use a simple ensemble strategy:

$$y^{pred} = 0.5 * (p_\phi(y|x_0) + p_\phi(y|x^{TT})), \quad (14)$$

where  $y^{pred}$  is the final prediction of the label by the classifier.

Algorithm 1 summarizes the entire method. Based on the proposed method, we aim to alleviate the semantic information loss caused by data shift and alleviate model shift.

---

**Algorithm 1** The overall algorithm for GDDA

---

**Input:**  $x^{TT}, T, \epsilon_\theta, \sigma(\cdot), p_\phi(y|x)$  ▷ Pre-trained diffusion model  
**Output:**  $y^{pred}$

- 1:  $x_T \sim \mathcal{N}(0, 1)$
- 2: Generate  $x^{blk}$  and  $x^{whi}$  by Eq. 13
- 3: **for**  $t$  in  $[T, T - 1, \dots, 1]$  **do**
- 4:     Calculate  $\hat{x}_t$  and  $x_{t-1}$  by Eq. 4
- 5:     **if** Eq. 13 **then**
- 6:         Calculate  $g^1$  by Eq. 10
- 7:          $g^2 \leftarrow \nabla_{x_t} \|\hat{x}_t - x^{TT}\|_2^2$  by Eq. 11
- 8:          $g^3 \leftarrow \nabla_{x_t} \ell_{LPIPS}(\hat{x}_t, x^{TT})$  by Eq. 12
- 9:          $x_{t-1} \leftarrow x_{t-1} - g^1 - g^2 - g^3$
- 10:     **else**
- 11:          $x_{t-1} \leftarrow x_{t-1}$
- 12:     **end if**
- 13: **end for**

Calculate  $y^{pred}$  by Eq. 14  
**Return:**  $y^{pred}$

---

Table 1: Classification accuracy(%) against the different types of corruption on CIFAR-10C under WideResNet28-10, where Gaussian-B is the Gaussian blur corruption and Gaussian-N is the Gaussian noise.

Method	Brightness	Contrast	Defocus	Elastic	Fog	Frost	Gaussian-B	Gaussian-N	Glass	Impulse	JPEG	Motion	Pixel	Saturate	Shot	Snow	Spatter	Speckle	Zoom	Avg.
<b>Source-to-target</b>																				
MEMO [7]	93.53	90.74	88.95	81.25	90.74	85.6	85.04	72.43	60.04	61.27	65.4	74.0	68.42	73.44	55.25	57.14	57.59	48.88	54.02	71.78
TENT [3]	<b>95.05</b>	<b>88.8</b>	<b>90.89</b>	81.51	86.98	85.68	<b>85.94</b>	74.74	69.01	73.7	77.34	80.73	<b>84.11</b>	90.1	78.91	82.29	80.73	79.69	85.42	82.72
<b>Target-to-source</b>																				
DiffPure [18]	78.96	68.96	65.21	69.79	78.96	57.92	57.29	48.96	41.04	50.21	60.42	61.04	65.0	78.75	51.46	65.21	68.33	56.04	62.08	62.4
BackToSource [4]	83.63	76.18	76.47	72.55	80.29	64.8	63.63	55.49	53.24	55.39	68.73	67.55	68.04	81.08	63.04	69.22	75.59	60.0	68.04	68.58
GDDA(Our)	92.35	80.0	83.92	<b>86.47</b>	<b>87.06</b>	<b>89.22</b>	78.24	<b>82.75</b>	<b>72.25</b>	<b>78.04</b>	<b>84.31</b>	<b>82.45</b>	82.45	<b>92.45</b>	<b>83.33</b>	<b>85.88</b>	<b>90.39</b>	<b>85.39</b>	<b>80.49</b>	<b>84.08</b>

## 5 Experiment

### 5.1 Experiment Settings

**Datasets and network architectures.** We consider three datasets for evaluation: CIFAR-10C, CIFAR-100C, and ImageNetC [28]. Meanwhile, we compare various state-of-the-art target-to-source methods such as BacktoSource [4] and DiffPure [18]. To show the improvement of our method, we also compare various state-of-the-art source-to-target methods such as Tent [3] and MEMO [7]. For pre-trained classifiers, we consider two widely used backbones for CIFAR-10C and CIFAR-100C: WideResNet-28-10 [1] and ResNet26 [29]. For ImageNet, we consider the ResNet50 [29] as the backbone.

**Diffusion model settings.** We use the unconditional CIFAR-10 checkpoint of EDM offered by NVIDIA [30] for our method on CIFAR-10C datasets. We fine-tune the unconditional CIFAR-10 checkpoint based on CIFAR-100 for CIFAR-100C following the training method offered by NVIDIA [30]. For ImageNetC, we use the pre-trained diffusion model offered by Dhariwal *et al.* [31]. We evaluate our model on a single RTX4090 GPU with 24GB memory. To prove

Table 2: Classification accuracy(%) against the different types of corruption on CIFAR-10C under ResNet26, where Gaussian-B is the Gaussian blur corruption and Gaussian-N is the Gaussian noise.

Method	Brightness	Contrast	Defocus	Elastic	Fog	Frost	Gaussian-B	Gaussian-N	Glass	Impulse	JPEG	Motion	Pixel	Saturate	Shot	Snow	Spatter	Speckle	Zoom	Avg.
<b>Source-to-target</b>																				
MEMO [7]	88.73	82.03	86.16	79.46	82.81	75.45	79.13	63.84	52.46	54.91	65.85	70.54	60.94	66.52	49.89	47.99	47.66	37.95	40.29	64.87
TENT [3]	86.98	<b>83.85</b>	<b>86.46</b>	80.47	83.33	82.03	<b>82.03</b>	70.57	70.05	72.14	77.08	<b>83.85</b>	78.91	85.94	75.52	76.3	80.99	77.6	84.64	79.93
<b>Target-to-source</b>																				
DiffPure [18]	77.5	62.29	64.17	61.88	70.42	57.71	56.67	46.25	40.42	52.71	61.46	57.29	61.04	75.63	52.92	65.0	67.92	55.83	57.5	60.24
BackToSource [4]	88.4	63.2	75.2	76.8	82.4	74.2	68.0	73.0	64.4	75.2	78.8	71.2	81.0	84.0	76.4	72.4	80.8	79.4	67.2	75.37
GDDA(Our)	<b>89.2</b>	<b>68.44</b>	<b>77.2</b>	<b>75.33</b>	<b>80.0</b>	<b>84.4</b>	<b>70.4</b>	<b>83.78</b>	<b>68.0</b>	<b>84.89</b>	<b>83.33</b>	<b>71.4</b>	<b>79.2</b>	<b>87.8</b>	<b>87.0</b>	<b>81.11</b>	<b>82.8</b>	<b>86.2</b>	<b>68.8</b>	<b>79.96</b>

the proposed guidance method could work with the accelerating sampling method for the diffusion model, we directly implement our method based on the DPM-Solver++ [26]. For CIFAR-10C and CIFAR-100C, we use  $T = 70$ , and for ImageNetC we use  $T = 75$ .

**Evaluation metrics.** Similar to the Gao *et al.* [4], we evaluate our method based on the accuracy under nineteen types of corruptions [28] such as brightness and fog. Meanwhile, to reduce the computation cost, we evaluate the accuracy of our method and previous works on a fixed subset of 500 images randomly sampled from the test set for each type of corruption similar to Nie *et al.* [18].

## 5.2 Experimental Results

**CIFAR-10C.** Table. 1 reports the experimental results against the 19 types of corruption on CIFAR-10C using WideResNet28-10 backbone. Compared with the state-of-the-art target-to-source methods, our model improves the classification accuracy of all types of corruption. Concretely, GDDA improves by at least 3.18% in contrast corruption. Additionally, it achieves a significant improvement of 27.26% on Gaussian noise corruption. Meanwhile, the GDDA achieves 16.3% average accuracy improvements, which proves the validity of the proposed methods. In the end, compared with the Tent, our method successfully reduces the gap between the target-to-source and source-to-target methods, where our method even improves 1.3% average accuracy. These results demonstrate that GDDA could alleviate the data shift and model shift to improve the accuracy of the classifier in TTA on CIFAR-10C dataset.

Table 3: Classification accuracy(%) against the different types of corruption on CIFAR-100C under WideResNet28-10, where Gaussian-B is the Gaussian blur corruption and Gaussian-N is the Gaussian noise.

Method	Brightness	Contrast	Defocus	Elastic	Fog	Frost	Gaussian-B	Gaussian-N	Glass	Impulse	JPEG	Motion	Pixel	Saturate	Shot	Snow	Spatter	Speckle	Zoom	Avg.
<b>Source-to-target</b>																				
MEMO [7]	<b>89.62</b>	<b>83.37</b>	<b>84.15</b>	<b>77.46</b>	<b>83.82</b>	<b>73.55</b>	<b>78.68</b>	<b>63.28</b>	<b>52.34</b>	52.34	57.48	63.73	56.25	60.83	39.96	41.18	39.29	31.36	36.27	61.31
TENT [3]	74.22	64.58	72.92	62.76	66.15	63.02	62.24	44.27	49.48	45.05	47.4	60.42	<b>60.68</b>	58.85	48.96	55.21	57.81	49.74	<b>61.2</b>	58.16
<b>Target-to-source</b>																				
DiffPure [18]	56.46	38.13	44.58	40.42	48.33	34.79	35.21	21.04	20.21	23.54	28.75	37.08	38.54	53.33	24.38	40.83	43.33	25.0	40.42	36.55
BackToSource [4]	40.2	31.86	46.86	41.37	29.22	32.35	43.43	40.29	42.84	38.92	43.82	43.73	43.04	45.39	44.41	37.94	41.76	39.31	44.22	40.58
GDDA(Our)	71.56	53.53	64.02	60.0	63.43	61.27	55.49	55.78	41.78	<b>56.89</b>	<b>59.33</b>	60.29	<b>55.2</b>	<b>62.84</b>	<b>65.11</b>	<b>59.12</b>	<b>64.31</b>	<b>63.33</b>	61.11	<b>59.63</b>

To further demonstrate the effectiveness of our method on different backbones, Table. 2 reports the experimental results under the ResNet26 backbone. Compared with BackToSource and TENT, our method achieves an average accuracy improvement of almost 3% and only has a gap of 1% respectively. Compared with the MEMO, our method achieves an average accuracy improvement of almost 15.09%. This demonstrates that GDDA could improve the performance of various backbones.

**CIFAR-100C.** Table. 3 reports the experimental results against the 19 types of corruption on CIFAR-100C using WideResNet28-10 backbone. Compared with the BackToSource, we have achieved an average accuracy improvement of 16.99%. It can be observed that we improved accuracy in all types of corruption compared with the BackToSource. This first demonstrates that there are weaknesses in the target-to-source method, specifically related to data shift and model shift. Then, it also proves that GDDA could mitigate these weaknesses through the implementation of detail guidance, global guidance, and class-aware guidance. Meanwhile, Compared with the target and parameter-based methods, we reduce the gap of average accuracy from 17.58% to 0.59%. In cases of challenging corruption that result in significant semantic information loss, such as Speckle and Gaussian noise, GDDA improves accuracy by almost 11%. This further confirms the effectiveness of GDDA.

**ImageNetC.** Table. 4 reports the experimental results against the 19 types of corruption using the ResNet50 backbone on 5-level severity corruption. We utilize the DPM-Solver++ acceleration sampling method to complete the entire ImageNetC experiment in just 75 timesteps. This showcases the potential of our work. Firstly, when compared with BackToSource, GDDA shows an improvement in average accuracy of 11.63%. Meanwhile, compared with the best result of TENT under various batch sizes, we even improved the 1.63% average accuracy, which further proves the validity of GDDA and the potential ability to deal with the domain shift for test-time adaptation. It can also be noted that GDDA still gets the best average accuracy compared with the source-to-target methods in various batch sizes. The large improvement is from the noise corruption, which further demonstrates our arguments that label semantic loss caused by the data shift is the key factor for the target-to-source methods.

To sum up, we report the experimental results of GDDA against 19 types of corruption among three datasets. Compared with the target-to-source methods. GDDA achieves large improvement among all datasets against 19 types of corruption. Meanwhile, to further prove the effectiveness, we report the experimental results compared with the latest source-to-target methods. According to the results, GDDA could reach a close performance and even make a few improvements



Table 4: Classification accuracy(%) against the different types of corruption on ImageNetC under ResNet50, where Gaussian-B is the Gaussian blur and Gaussian-N is the Gaussian noise. Source-to-target (N) means the source-to-target method using N batch size.

Method	Brightness	Contrast	Defocus	Elastic	Fog	Frost	Gaussian-B	Gaussian-N	Glass	Impulse	JPEG	Motion	Pixel	Saturate	Shot	Snow	Spatter	Speckle	Zoom	Avg.
<b>Source-to-target (N)</b>																				
MEMO(N=64)	67.41	12.28	14.96	47.54	53.79	47.54	12.28	14.29	15.18	18.08	34.38	25.67	42.86	64.29	11.83	41.52	38.84	33.48	37.5	33.35
MEMO(N=100)	<b>70.67</b>	19.33	16.0	<b>53.33</b>	58.67	42.0	10.67	16.0	<b>20.67</b>	12.67	38.67	24.0	42.0	<b>65.33</b>	13.33	43.33	38.0	32.0	38.67	34.49
TENT(N=64)	68.97	15.85	<b>16.96</b>	46.65	53.57	40.4	10.27	15.4	17.63	17.63	40.18	<b>34.82</b>	43.53	66.29	15.62	<b>47.32</b>	42.41	36.61	43.08	35.43
TENT(N=100)	70.31	13.28	13.54	47.92	<b>61.72</b>	48.18	10.94	15.62	17.45	15.89	35.16	32.29	43.23	65.36	21.35	45.31	40.36	33.59	42.71	35.48
TENT(N=128)	70.09	12.5	16.07	48.21	58.48	48.88	<b>14.29</b>	17.41	20.09	16.29	37.05	30.8	45.09	59.38	20.98	42.63	<b>46.65</b>	35.04	<b>43.97</b>	35.99
<b>Target-to-source</b>																				
DiffPure [18]	58.16	16.33	8.16	18.37	33.67	26.53	8.16	5.1	7.14	11.22	41.84	14.29	30.61	62.24	7.14	26.53	22.45	23.47	26.53	23.58
BackToSource [4]	55.1	15.31	6.12	21.43	38.78	22.45	9.18	22.45	12.24	11.22	41.84	16.33	27.55	55.1	26.53	18.37	38.78	32.65	<b>22.45</b>	25.99
GDDA(Our)	65.31	<b>20.41</b>	10.2	38.78	31.31	<b>53.54</b>	9.09	<b>54.55</b>	17.17	<b>45.45</b>	<b>52.04</b>	20.2	<b>47.47</b>	63.64	<b>44.44</b>	31.63	44.9	<b>49.49</b>	15.15	<b>37.62</b>

in part of corruption, especially for the noise type corruption including Gaussian noise and impulse noise. In the end, the acceleration method could be used to improve the sampling speed of GDDA, we use the DPM-Solver to complete the experiments on the ImageNetC. In this condition, GDDA still achieves state-of-the-art performance compared with the latest target-to-source method. This demonstrates the feasibility of the GDDA.

### 5.3 Ablation Study

$g^1$	$g^2$	$g^3$	Sam	Avg.(%)
✓			✓	17.51
	✓		✓	22.56
		✓	✓	10.89
✓	✓		✓	31.58
✓	✓	✓	✓	28.03
✓	✓	✓	✓	37.62

Table 5: Ablation study for GDMA based on ImageNetC with ResNet50, where Sam is the sampling strategy.

To show the effectiveness of our method we report the ablation study for the combinations of the guidance. We also report more ablation studies including two hyperparameters  $\eta$  for  $g^2$  and  $t^*$  for  $g^1$ , the influence of the ensemble strategy, and the influence of the batch size in supplementary.

**Guidance.** To prove the effectiveness of the proposed guidance, we report the ablation study for the combination of the guidance reported in Table 5. It can be shown that using each guidance alone will decrease the performance of the GDDA. Meanwhile, we also want to prove the necessity of the sampling strategy, especially under the acceleration method. It can be shown that the sampling strategy improves almost 9% average accuracy, which shows that the accumulating error will be aggravated by the DPM-Solver++ and thus lead the low-quality generation. We also report visualization results under the supplementary to further support this view.

## 6 Conclusion

We proposed the guidance-based diffusion-driven adaptation. By leveraging the feature embedding from both the classifier and the diffusion model, we show the potential for the target-to-source methods and alleviate the gap between target-to-source methods and source-to-target methods. The experimental results demonstrate that GDDA gets state-of-the-art results compared with the latest target-to-source methods. Meanwhile, compared with the latest source-to-target methods, our method gets a better result for some types of corruption and even the average accuracy in CIFAR-10C, CIFAR-100C, and ImageNetC with different backbones. Meanwhile, for the difficult ImageNetC with 5-level severity, we achieve state-of-the-art performance based on the DPM-Solver++.

We also report the other findings in our work: 1) The acceleration method is sensitive to the gradient of guidance, which makes it difficult to implement the guidance method directly on the entire reverse process. 2) The target-to-source techniques are not particularly effective for blurring type corruptions mentioned in the supplementary material. We will further explore this condition.

## References

- [1] Sergey Zagoruyko and Nikos Komodakis. Wide residual networks. In Richard C. Wilson, Edwin R. Hancock, and William A. P. Smith, editors, *Proceedings of the British Machine Vision Conference 2016, BMVC 2016, York, UK, September 19-22, 2016*. BMVA Press, 2016.
- [2] Junjiao Tian, Lavisha Aggarwal, Andrea Colaco, Zsolt Kira, and Mar González-Franco. Diffuse, attend, and segment: Unsupervised zero-shot segmentation using stable diffusion. *CoRR*, abs/2308.12469, 2023.
- [3] Dequan Wang, Evan Shelhamer, Shaoteng Liu, Bruno A. Olshausen, and Trevor Darrell. Tent: Fully test-time adaptation by entropy minimization. In *9th International Conference on Learning Representations, ICLR 2021, Virtual Event, Austria, May 3-7, 2021*, 2021.
- [4] Jin Gao, Jialing Zhang, Xihui Liu, Trevor Darrell, Evan Shelhamer, and Dequan Wang. Back to the source: Diffusion-driven adaptation to test-time corruption. In *IEEE/CVF Conference on Computer Vision and Pattern Recognition, CVPR 2023, Vancouver, BC, Canada, June 17-24, 2023*, pages 11786–11796, 2023.
- [5] Ian J. Goodfellow, Jonathon Shlens, and Christian Szegedy. Explaining and harnessing adversarial examples. In Yoshua Bengio and Yann LeCun, editors, *3rd International Conference on Learning Representations, ICLR 2015, San Diego, CA, USA, May 7-9, 2015, Conference Track Proceedings*, 2015.
- [6] Sachin Goyal, Mingjie Sun, Aditi Raghunathan, and J. Zico Kolter. Test time adaptation via conjugate pseudo-labels. In *NeurIPS*, 2022.
- [7] Marvin Zhang, Sergey Levine, and Chelsea Finn. MEMO: test time robustness via adaptation and augmentation. In *NeurIPS*, 2022.
- [8] Yu Sun, Xiaolong Wang, Zhuang Liu, John Miller, Alexei A. Efros, and Moritz Hardt. Test-time training with self-supervision for generalization under distribution shifts. In *Proceedings of the 37th International Conference on Machine Learning, ICML 2020, 13-18 July 2020, Virtual Event*, volume 119 of *Proceedings of Machine Learning Research*, pages 9229–9248. PMLR, 2020.
- [9] A. Tuan Nguyen, Thanh Nguyen-Tang, Ser-Nam Lim, and Philip H.S. Torr. Tipi: Test time adaptation with transformation invariance. In *Proceedings of the IEEE/CVF Conference on Computer Vision and Pattern Recognition (CVPR)*, pages 24162–24171, June 2023.
- [10] Liang Chen, Yong Zhang, Yibing Song, Ying Shan, and Lingqiao Liu. Improved test-time adaptation for domain generalization. In *Proceedings of the IEEE/CVF Conference on Computer Vision and Pattern Recognition (CVPR)*, pages 24172–24182, June 2023.
- [11] Yi-Fan Zhang, Jindong Wang, Jian Liang, Zhang Zhang, Baosheng Yu, Liang Wang, Dacheng Tao, and Xing Xie. Domain-specific risk minimization for domain generalization. In *Proceedings of the 29th ACM SIGKDD Conference on Knowledge Discovery and Data Mining, KDD 2023, Long Beach, CA, USA, August 6-10, 2023*, pages 3409–3421. ACM, 2023.
- [12] Shuaicheng Niu, Jiayang Wu, Yifan Zhang, Yafo Chen, Shijian Zheng, Peilin Zhao, and Mingkui Tan. Efficient test-time model adaptation without forgetting. In Kamalika Chaudhuri, Stefanie Jegelka, Le Song, Csaba Szepesvári, Gang Niu, and Sivan Sabato, editors, *International Conference on Machine Learning, ICML 2022, 17-23 July 2022, Baltimore, Maryland, USA*, volume 162 of *Proceedings of Machine Learning Research*, pages 16888–16905. PMLR, 2022.
- [13] Hao Zhao, Yuejiang Liu, Alexandre Alahi, and Tao Lin. On pitfalls of test-time adaptation. In Andreas Krause, Emma Brunskill, Kyunghyun Cho, Barbara Engelhardt, Sivan Sabato, and Jonathan Scarlett, editors, *International Conference on Machine Learning, ICML 2023, 23-29 July 2023, Honolulu, Hawaii, USA*, volume 202 of *Proceedings of Machine Learning Research*, pages 42058–42080. PMLR, 2023.
- [14] Jonathan Ho, Ajay Jain, and Pieter Abbeel. Denoising diffusion probabilistic models. In Hugo Larochelle, Marc’Aurelio Ranzato, Raia Hadsell, Maria-Florina Balcan, and Hsuan-Tien Lin, editors, *Advances in Neural Information Processing Systems 33: Annual Conference on Neural Information Processing Systems 2020, NeurIPS 2020, December 6-12, 2020, virtual*, 2020.
- [15] Minguk Kang and Jaesik Park. Contragan: Contrastive learning for conditional image generation. In Hugo Larochelle, Marc’Aurelio Ranzato, Raia Hadsell, Maria-Florina Balcan, and Hsuan-Tien Lin, editors, *Advances in Neural Information Processing Systems 33: Annual Conference on Neural Information Processing Systems 2020, NeurIPS 2020, December 6-12, 2020, virtual*, 2020.
- [16] Serin Yang, Hyunmin Hwang, and Jong Chul Ye. Zero-shot contrastive loss for text-guided diffusion image style transfer. *CoRR*, abs/2303.08622, 2023.

- [17] Richard Zhang, Phillip Isola, Alexei A. Efros, Eli Shechtman, and Oliver Wang. The unreasonable effectiveness of deep features as a perceptual metric. In *2018 IEEE Conference on Computer Vision and Pattern Recognition, CVPR 2018, Salt Lake City, UT, USA, June 18-22, 2018*, pages 586–595. Computer Vision Foundation / IEEE Computer Society, 2018.
- [18] Weili Nie, Brandon Guo, Yujia Huang, Chaowei Xiao, Arash Vahdat, and Animashree Anandkumar. Diffusion models for adversarial purification. In Kamalika Chaudhuri, Stefanie Jegelka, Le Song, Csaba Szepesvári, Gang Niu, and Sivan Sabato, editors, *International Conference on Machine Learning, ICML 2022, 17-23 July 2022, Baltimore, Maryland, USA*, volume 162 of *Proceedings of Machine Learning Research*, pages 16805–16827. PMLR, 2022.
- [19] Hyungjin Chung, Jeongsol Kim, Michael Thompson McCann, Marc Louis Klasky, and Jong Chul Ye. Diffusion posterior sampling for general noisy inverse problems. In *The Eleventh International Conference on Learning Representations, ICLR 2023, Kigali, Rwanda, May 1-5, 2023*. OpenReview.net, 2023.
- [20] Jiaming Song, Arash Vahdat, Morteza Mardani, and Jan Kautz. Pseudoinverse-guided diffusion models for inverse problems. In *The Eleventh International Conference on Learning Representations, ICLR 2023, Kigali, Rwanda, May 1-5, 2023*. OpenReview.net, 2023.
- [21] Narek Tumanyan, Michal Geyer, Shai Bagon, and Tali Dekel. Plug-and-play diffusion features for text-driven image-to-image translation. In *IEEE/CVF Conference on Computer Vision and Pattern Recognition, CVPR 2023, Vancouver, BC, Canada, June 17-24, 2023*, pages 1921–1930. IEEE, 2023.
- [22] Yang Song, Jascha Sohl-Dickstein, Diederik P. Kingma, Abhishek Kumar, Stefano Ermon, and Ben Poole. Score-based generative modeling through stochastic differential equations. In *9th International Conference on Learning Representations, ICLR 2021, Virtual Event, Austria, May 3-7, 2021*. OpenReview.net, 2021.
- [23] Alexey Dosovitskiy, Lucas Beyer, Alexander Kolesnikov, Dirk Weissenborn, Xiaohua Zhai, Thomas Unterthiner, Mostafa Dehghani, Matthias Minderer, Georg Heigold, Sylvain Gelly, Jakob Uszkoreit, and Neil Houlsby. An image is worth 16x16 words: Transformers for image recognition at scale. In *9th International Conference on Learning Representations, ICLR 2021, Virtual Event, Austria, May 3-7, 2021*. OpenReview.net, 2021.
- [24] Minguk Kang and Jaesik Park. Contragan: Contrastive learning for conditional image generation. In Hugo Larochelle, Marc’Aurelio Ranzato, Raia Hadsell, Maria-Florina Balcan, and Hsuan-Tien Lin, editors, *Advances in Neural Information Processing Systems 33: Annual Conference on Neural Information Processing Systems 2020, NeurIPS 2020, December 6-12, 2020, virtual*, 2020.
- [25] Laurent Valentin Jospin, Hamid Laga, Farid Boussaid, Wray Buntine, and Mohammed Bennamoun. Hands-on bayesian neural networks—a tutorial for deep learning users. *IEEE Computational Intelligence Magazine*, 17(2):29–48, may 2022.
- [26] Cheng Lu, Yuhao Zhou, Fan Bao, Jianfei Chen, Chongxuan Li, and Jun Zhu. Dpm-solver++: Fast solver for guided sampling of diffusion probabilistic models. *CoRR*, abs/2211.01095, 2022.
- [27] Jiwen Yu, Yinhuai Wang, Chen Zhao, Bernard Ghanem, and Jian Zhang. Freedom: Training-free energy-guided conditional diffusion model. *CoRR*, abs/2303.09833, 2023.
- [28] Dan Hendrycks and Thomas G. Dietterich. Benchmarking neural network robustness to common corruptions and perturbations. In *7th International Conference on Learning Representations, ICLR 2019, New Orleans, LA, USA, May 6-9, 2019*. OpenReview.net, 2019.
- [29] Kaiming He, Xiangyu Zhang, Shaoqing Ren, and Jian Sun. Deep residual learning for image recognition. In *2016 IEEE Conference on Computer Vision and Pattern Recognition, CVPR 2016, Las Vegas, NV, USA, June 27-30, 2016*, pages 770–778. IEEE Computer Society, 2016.
- [30] Tero Karras, Miika Aittala, Timo Aila, and Samuli Laine. Elucidating the design space of diffusion-based generative models. In *NeurIPS*, 2022.
- [31] Prafulla Dhariwal and Alexander Quinn Nichol. Diffusion models beat gans on image synthesis. In Marc’Aurelio Ranzato, Alina Beygelzimer, Yann N. Dauphin, Percy Liang, and Jennifer Wortman Vaughan, editors, *Advances in Neural Information Processing Systems 34: Annual Conference on Neural Information Processing Systems 2021, NeurIPS 2021, December 6-14, 2021, virtual*, pages 8780–8794, 2021.
- [32] Junjiao Tian, Lavisha Aggarwal, Andrea Colaco, Zsolt Kira, and Mar González-Franco. Diffuse, attend, and segment: Unsupervised zero-shot segmentation using stable diffusion. *CoRR*, abs/2308.12469, 2023.

## 7 Appendix

To show the effectiveness of GDDA, we report the additional visualization results.

Figure. 3 reports the visualization of GDDA compared with the target-to-source baselines. It was found that GDDA keeps the semantics as much as possible. In contrast to corruption, GDDA is able to recover part of the semantics. Meanwhile, in spatter corruption, GDDA is able to remove the extra noise and keep the label semantic, which proves the effectiveness of GDDA. Meanwhile, we also report the ablation study about the sampling strategy. It could be found that the sampling strategy could improve the quality of the generated image, which proves the necessity of the sampling strategy. Meanwhile, it also shows that the sampling strategy is also important for the acceleration method in target-to-source methods, which is an additional finding in our work.

**Hyperparameters.** GDDA contains two hyperparameters: the special time  $t$  for  $g^1$  and the small weight  $\eta$  for  $g^2$ . We report the influence of the hyperparameters on the quality of the generated images shown in Figure. 4 and Figure. 5 respectively. For special time  $t$ , previous works [16, 32] show that the diffusion model will tend to focus on the local details when the  $t$  tends to be 0. However, the extra noise introduced by the corruption such as the impulse noise will influence the generated images if we directly set  $t = 0$ . In this condition, we slightly increase the  $t$  to let the diffusion model focus on the local details and ignore part of the noise. As shown in Figure. 4, when  $t = 0.1$ , the diffusion model starts to drop the local detail since it can be found that the quality of the generated image against contrast is decreasing. In internal  $t \in [0.05, 0.008]$ , the generated images have a high quality compared with the interval  $t \in [0.007, 0.005]$ . Therefore, choosing the value in internal  $[0.05, 0.008]$  can get a great result. In our work, we directly set  $t = 0.008$ .

We also report the influence of  $\eta$  shown in Figure. 5. Firstly, it can be found that it is necessary to use the  $g^2$  to keep the overall style. When  $\eta = 0$ , the generated images have low quality. By increasing the  $\eta$  slightly, the image quality will increase. However, with the increasing of the  $\eta$ , the defect of the MSE will introduce extra noise, since corruption will break the label semantic and have a negative influence on the generated images. In this condition, we just set  $\eta$  in  $[0.01, 0.03]$  interval to avoid introducing too much corruption, whereas in our work we use  $\eta = 0.02$ .

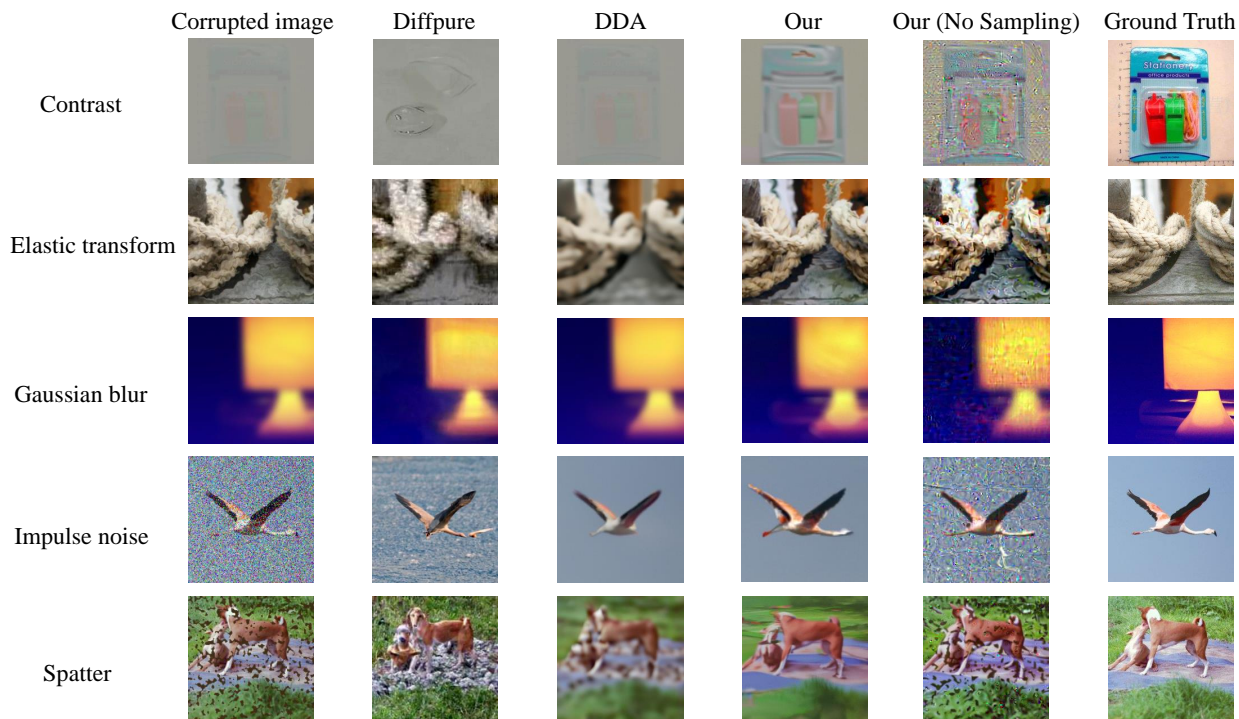


Figure 3: Visualization of ablation study for different models against different corruption, where our (no sampling) means we do not use the proposed sampling strategy and ground truth is the image without corruption.

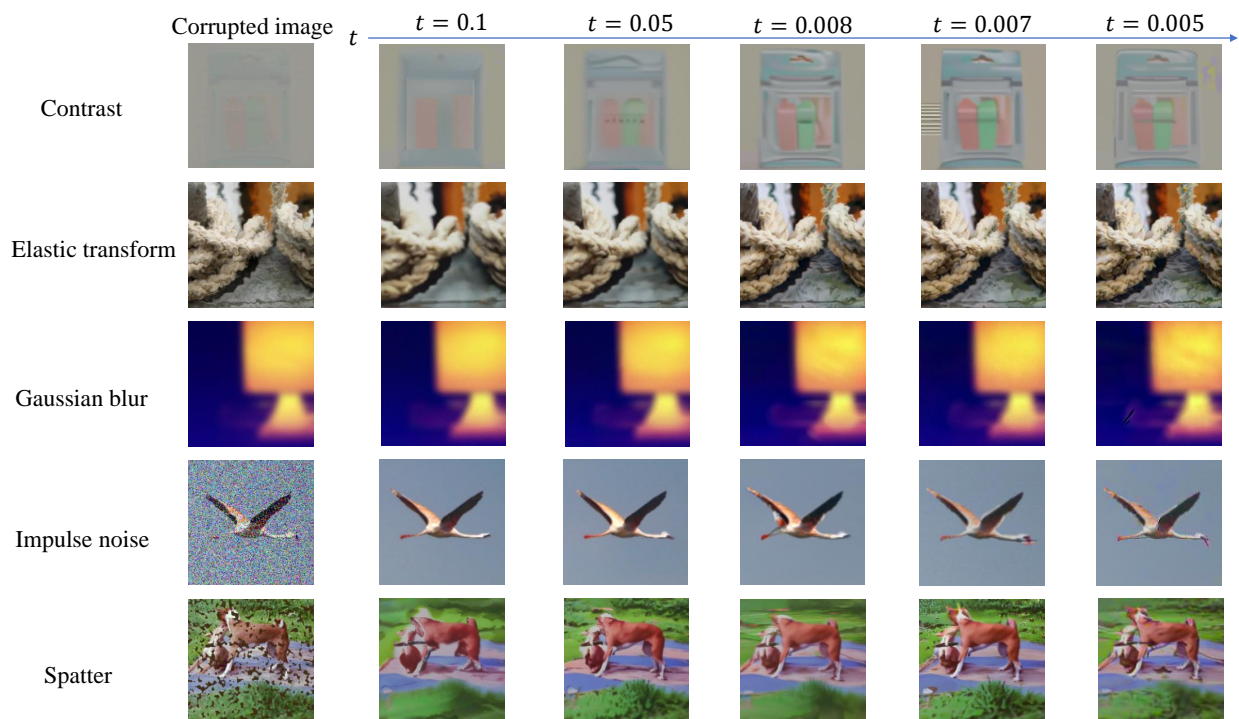


Figure 4: Visualization of ablation study for  $t$  in  $g^1$  against different corruption.

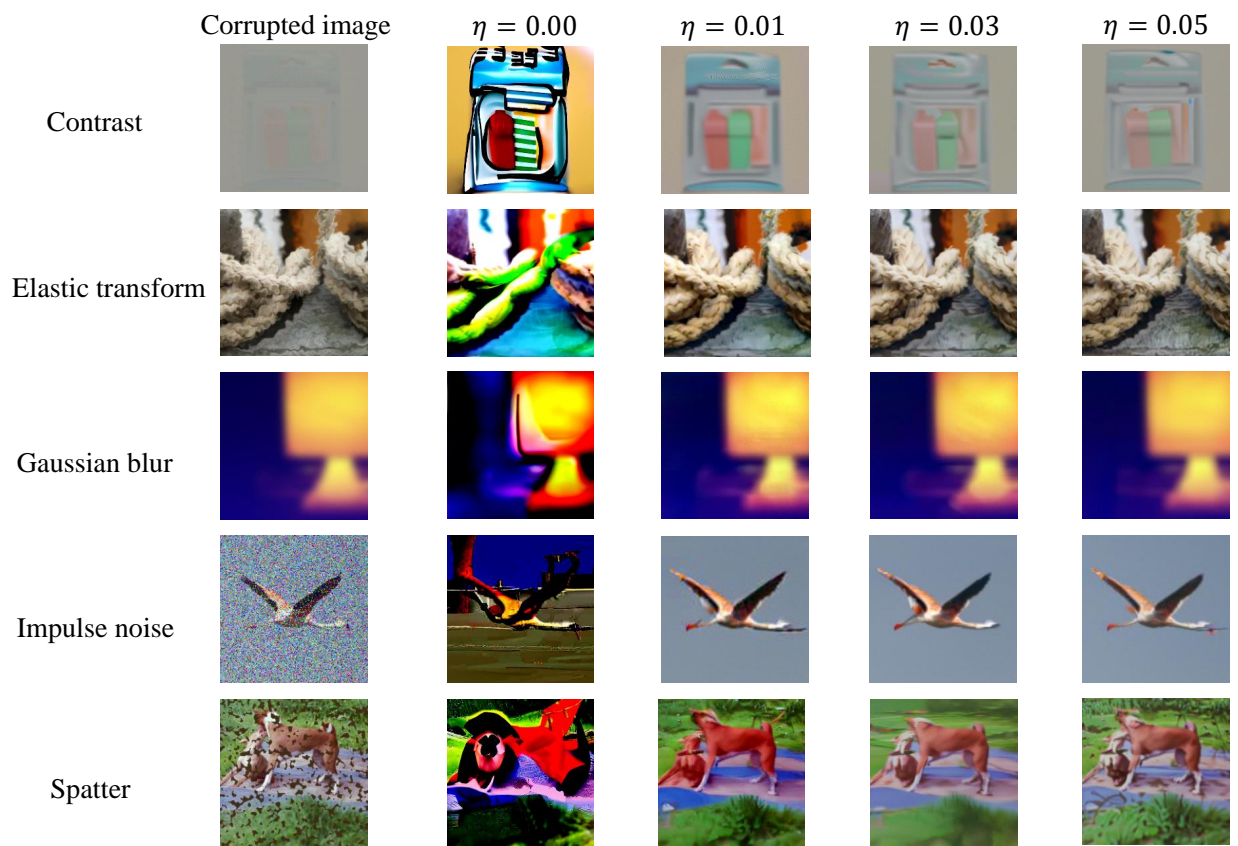


Figure 5: Visualization of ablation study for  $\eta$  in  $g^2$  against different corruption.